Unusual Geometries and Questions of Oxidation State in Potential Sn(III) Chemistry

Pradeep Gutta and Roald Hoffmann*

Department of Chemistry and Chemical Biology, Baker Laboratory, Cornell University, Ithaca, New York 14853-1301

A mixed-valence compound ($Sn_2I_3(NPPh_3)_3$) with nonequivalent Sn atoms in characteristic 2+ and 4+ Sn geometries, raised the idea of an average Sn^{3+} structure. The extended structures of $Sr_4Sn_2Se_9$ and $Sr_4Sn_2Se_{10}$ contain an unusual Sn_2Se_6 subunit, which has two equal Se–Sn–Se angles close to 160°. This was suggestive of a Sn^{3+}/Sn^{3+} compound, similar to the putative transition state for the valence state interchange in the molecular compound. These interesting geometrical features of two quite different molecules prompt a series of computations, a detective story of geometries and oxidation states, which concludes tentatively that the Sn with the abnormal angle in the extended structure is still likely to be formally Sn^{4+}.

Commonly known oxidation states of tin are 0, 2+, and 4+. The 3+ oxidation state occurs primarily in compounds having a Sn–Sn single bond. Our interest in this unusual oxidation state in the absence of Sn–Sn bonding was stimulated by two seemingly very different structures reported recently.

A Molecular Compound, Clearly Sn^{2+}/Sn^{4+}

The first structure is that of $Sn_2I_3(NPPh_3)_3$ (Figure 1), clearly a mixed-valence molecular compound of tin.[1] The NPR_3 ligands in this molecule are unusual, so a word is needed on how one might count their electrons to reach a Sn oxidation state assignment. The ligand is similar to a neutral phosphine oxide, R_3PO. This makes it reasonable to view NPR_3 as mononegative. Three $(NPR_3)^{1-}$ ligands and three iodides imply a total of six formal positive charges to be distributed between the two tin atoms. Clearly an equal distribution, assigning 3+ to each tin, is questionable, as they are not geometrically equivalent. Sn_a in $Sn_2I_3(NPPh_3)_3$ is approximately tetrahedral, the range of angles between the ligands around it being between 86° and 117°. The coordination geometry of Sn_b is very different. One angle, I–Sn_b-I, is 176°, and the general coordination environment is SF_4-like, i.e., approximately a "trigonal bipyramid minus one". It then makes sense to assign to Sn_a oxidation state Sn^{4+}, and to Sn_b Sn^{2+}. The Sn^{2+}–I distances are longer (at 3.13
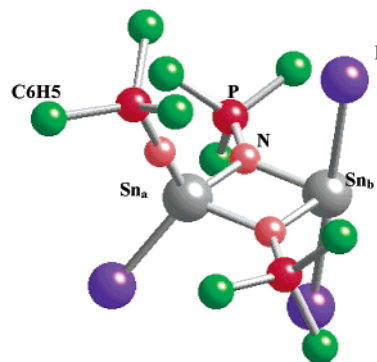

Figure 1. The structure of $Sn_2I_3(NPPh_3)_3$, a mixed-valence compound, with Sn^{4+} (Sn_a) and Sn^{2+} (Sn_b).

and 3.16 Å) than the Sn^{4+}–I distance of 2.67 Å, which is in accord with expectations for three-center electron-rich vs normal Sn–I bonding.

The two tin centers in $Sn_2I_3(NPPh_3)_3$ are clearly different. Yet they are bound in proximity to each other in a planar four-membered ring, connected by identical NR ligands. The structure immediately suggests the question: Could the two Sn centers, in different oxidation states, interconvert? What might be the mechanism and reaction barrier to such a process? A least-motion concerted interconversion mechanism that first comes to mind proceeds via a D_{2h} structure (if the ligands were identical), as indicated in Figure 2.

Some Extended Sn Structures with Geometries Suggestive of Sn^{3+}

While we were thinking about this possibility, we encountered the extended structures $Sr_4Sn_2Se_9$ and $Sr_4Sn_2Se_{10}$

* Author to whom correspondence should be addressed. E-mail: rh34@cornell.edu.

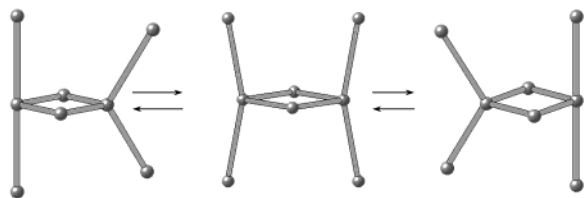(1) Chitsaz, S.; Neumüller, B.; Dehnicke, K. *Z. Anorg. Allg. Chem.* **2000**, *626*, 813–815.

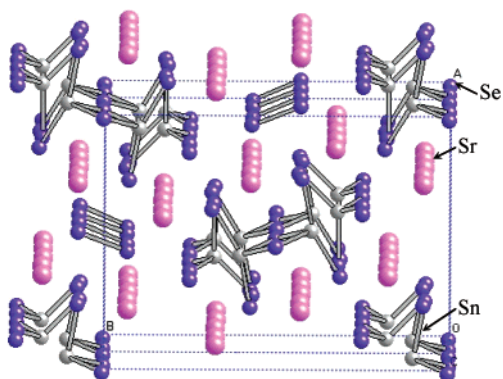**Figure 2.** A possible intercoversion of a Sn^{2+}/Sn^{4+} dimer though a D_{2h} structure.

Figure 3. $Sr_4Sn_2Se_9$, showing Se_2, $SnSe_4$, and Sn_2Se_6 subunits. One Sn_2Se_6 and two $SnSe_4$ units are seen alternating in the middle and at the edges of the cell (note: only one of the edges shows the full subunit structure).
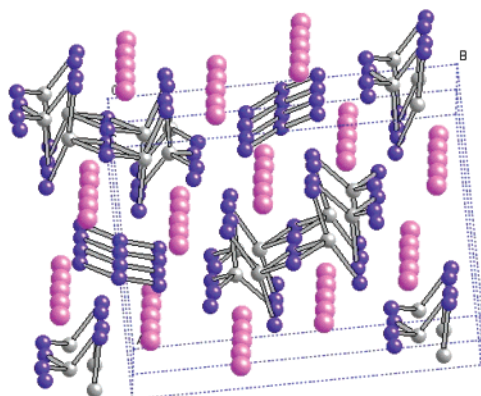

Figure 4. The crystal structure of $Sr_4Sn_2Se_{10}$, similar to $Sr_4Sn_2Se_9$, but containing Se_3 subunits.

(Figures 3 and 4).[2] These appear very different from the molecular compound in Figure 1, yet, as we will see, they are related. In the extended structures, the Se occurs in several forms, prominently featuring a Sn_2Se_6 subunit. Actually many such compounds have been reported.[3−11] The Sn_2Se_6 subunit in $Sr_4Sn_2Se_9$ and $Sr_4Sn_2Se_{10}$, however, differs

(2) Pocha, R.; Johrendt, D. Private communication.
(3) Sheldrick, W. S.; Braunbeck, H. G. *Z. Naturforsch., B: Chem. Sci.* **1989**, *44* (7), 851−852.
(4) Sheldrick, W. S.; Braunbeck, H. G. *Z. Anorg. Allg. Chem.* **1993**, *619* (7), 1300−1306.
(5) Sheldrick, W. S.; Sahaaf, B. *Z. Anorg. Allg. Chem.* **1994**, *620* (6), 1041−1045.
(6) Loose, A.; Sheldrick, W. S. *Z. Anorg. Allg. Chem.* **1999**, *625* (2), 233−240.
(7) Fehlker, A.; Blachnik, R. *Z. Anorg. Allg. Chem.* **2001**, *627* (3), 411−418.
(8) Guo, H.; Li, Z.; Yang, L.; Wang, P.; Huang, X.; Li, J. *Acta Crystallogr., Sect. C* **2001**, *C57* (11), 1237−1238.
(9) Borrmann, H.; Pirani, A. M.; Schrobilgen, G. J. *Acta Crystallogr.* **1997**, *C53*, 1004−1006.
(10) Eisenmann, B.; Hansa, J. *Z. Kristallogr.* **1993**, *203*, 299−302.
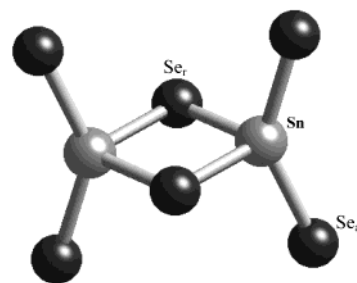(11) Krebs, B.; Uhlen, H. *Z. Anorg. Allg. Chem.* **1987**, *549*, 35−45.

Figure 5. A typical $Sn_2Se_6^{4-}$ subunit, as in $K_4Sn_2Se_6$ and $Cs_4Sn_2Se_6$.[3,10]

from more typical Sn_2Se_6 subunits,[3−11] which may be seen in compounds such as $K_4Sn_2Se_6$ and $Cs_4Sn_2Se_6$ (Figure 5).[3,10]

In a more typical $Sn_2Se_6^{4-}$ subunit one finds the following:

(1) A four-membered ring of alternating Sn and Se_r. The ring is generally planar, with $Se_r-Sn-Se_r$ being slightly greater than 90° (93−96°). The $Sn-Se_r$ distance is around 2.65 Å. The Sn−Sn distance ranges from 3.45 to 3.65 Å.

(2) Two terminal seleniums (Se_a) are bound to each of the above tins, making the geometry around the tin close to tetrahedral. The $Se_a-Sn-Se_a$ angles range from 104° to 127°. The plane of the $Se_a-Sn-Se_a$ is perpendicular to the plane of the $Sn-Se_r-Sn-Se_r$ ring.

(3) Since there is no Se−Se bonding, the seleniums may be formally counted as 2−. If the tins are counted as 4+, which would be consistent with the near-tetrahedral geometry, one comes to the 4− charge on the typical Sn_2Se_6 subunit. This assignment is consistent with normal counter-cation charge assignment, as in $K_4Sn_2Se_6$ and $Cs_4Sn_2Se_6$.[3,10]

In contrast to such typical structures, the Sn_2Se_6 subunits in $Sr_4Sn_2Se_9$ and $Sr_4Sn_2Se_{10}$ have $Se_a-Sn-Se_a$ angles around 160°. This is certainly a large departure from the "normal" tetrahedral angle, but still different from the 184° at the Sn^{2+} in the mixed-valence compound. Could the Sn in these unusual phases be Sn^{3+}? The geometry also looks like the putative transition state for the $Sn^{2+}-Sn^{4+}$ interchange (Figure 2), which came to mind while thinking about our first set of molecular compounds.

If we were to assume the tins in 3+ oxidation states instead of the 4+ assigned in the literature,[2] then the formal charge on the subunit should be 6− instead of 4−. The two extra electrons would have to come from another part of the structure. We will return to this point below.

These two structures led us to a general examination of the electronic structure and bonding in Sn_2X_6 systems.

Computational Methods

The Amsterdam Density Functional ADF2002.02 program was employed in our DFT computations.[12] A B-P86 functional, which combines Becke's GGA functional for exchange with Perdew's GGA functional for correlation, was utilized.[13−15] The triple-ζ basis sets of Slater type orbitals, which included a polarization function

(12) Velde, G. te; Bickelhaupt, F. M.; Baerends, E. J.; Guerra, C. F.; van Gisbergen, S. J. A.; Snijders, J. G.; Ziegler, T. *J. Comput. Chem.* **2001**, *22*, 931−967.
(13) Becke, A. D. *Phys. Rev. A* **1988**, *38*, 3098−3100.
(14) Perdew, J. P. *Phys. Rev. B* **1986**, *33*, 8822−8824.
(15) Perdew, J. P. *Phys. Rev. B* **1986**, *34*, 7406.

for all the atoms in the models, was employed to represent the valence orbitals. These basis sets were obtained from the ADF database.

Extended Hückel calculations were performed using CACAO and YAeHMOP programs.[16-18] Default parameters (Appendix 1), the same in both these packages for all the elements of concern, were used in our computations.

Models, Results, and Discussions

1. DFT Calculations on Cluster Models. 1.1. A $Sn^{4+}-Sn^{4+}$ System. To model a $Sn^{4+}-Sn^{4+}$ system we need a $Sn_2Se_6^{4-}$ ion. DFT computations with a 4− charge on the Sn_2Se_6 yielded greatly elongated and unrealistic $Sn-Se_r$ and $Sn-Se_a$ bonds. This might be expected, since the extra negative charges on the molecule, uncompensated by counterions, create an unbalanced charge distribution. To overcome this problem we added four potassiums, coming to a neutral $Sn_2Se_6K_4$ model. The placement of potassiums corresponds to the some of the strontium positions around the $Sn_2Se_6^{4-}$ subunit, in the crystal structures of $Sr_4Sn_2Se_9$ and $Sr_4Sn_2Se_{10}$.[2]

When the geometry of $Sn_2Se_6K_4$ was optimized, we obtained the structure of symmetry D_{2h} shown in Figure 6 (confirmed computationally to be a minimum). The computed $Se_a-Sn-Se_a$ angle of 143° is much opened from a tetrahedral geometry, and not that far from 160°, which was observed for Sn^{4+} in the crystal structures we mentioned.[2] The Se_a-Sn bond lengths in the computed model are 2.59 Å. The $Sn-Sn$ distance was 3.65 Å.

We then tried a model for the $Sn^{4+}-Sn^{2+}/Sn^{3+}-Sn^{3+}$ system.

1.2. $Sn^{4+}-Sn^{2+}/Sn^{3+}-Sn^{3+}$ Models. Optimizing the geometry of $Sn_2Se_6K_4^{2-}$, keeping D_{2h} symmetry, we obtain a structure not much different from that shown in Figure 6 for $Sn_2Se_6K_4$, except that the $Se_a-Sn-Se_a$ angle is 152° and the Se_a-Sn bond length 2.87 Å.

One small imaginary frequency was observed, which corresponded to the unsymmetrical angular motion of the angles of concern to us ($Se_a-Sn-Se_a$). We proceeded to optimize $Sn_2Se_6K_4^{2-}$ in lower symmetry (C_s), and obtained the structure shown in Figure 7. This structure is computationally confirmed to be a minimum. The two tin centers are now in quite different environments. The angles $Se_a-Sn1-Se_a$ and $Se_a-Sn2-Se_a$ are 167° and 133°, respectively. The Se_a-Sn1 and Se_a-Sn2 bond lengths are 3.07 Å and 2.64 Å, respectively, the differential being as expected for the two Sn bonding modes. The observed C_{2v} minimum is 0.16 eV below the D_{2h} geometry, a difference that could certainly be overcome by packing energies.

We return to the question of oxidation states and the unusual $Se_a-Sn-Se_a$ angles. The computed $Sn_2Se_6K_4^{0/2-}$ model compounds both have large $Se_a-Sn-Se_a$ angles. In the model for $Sn^{4+}-Sn^{4+}$ the angle is 144°; it opens up to

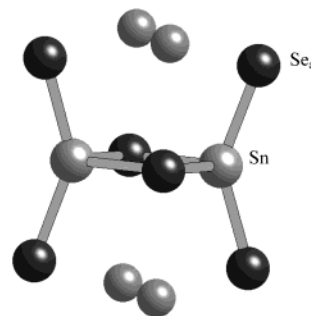(16) Mealli, C.; Proserpio, D. M. *J. Chem. Educ.* **1990**, *67*, 399–402.
(17) Mealli, C.; Ienco, A.; Proserpio, D. M. *Book of Abstracts of the XXXIII ICCC*', Florence, Italy, 1998, 510.
(18) Landrum, G. A.; Glassey, W. V, bind 3.0. bind is a part of the YAeHMOP package, which is available free of charge from http://sourceforge.net/projects/yaehmop.

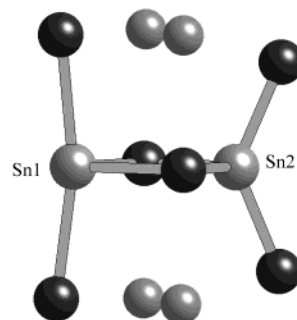**Figure 6.** Optimized geometry of $Sn_2Se_6K_4$. The $Se_a-Sn-Se_a$ angle is 144°.

Figure 7. Optimized geometry of $Sn_2Se_6K_4^{2-}$.

152° for $Sn^{3+}-Sn^{3+}$, which is closer to the 160° in the observed Pocha and Johrendt phases. But the computed $Sn-Se_a$ distances in the $Sn^{4+}-Sn^{4+}$ model (2.59 Å) are in much better accord with the $Sn-Se_a$ separation in the known unusual compounds (2.51–2.55 Å) than the $Sn^{3+}-Sn^{3+}$ model $Sn-Se_a$ (2.87 Å). The longer $Sn-Se_a$ bond in $Sn^{3+}-Sn^{3+}$ model (2.87 Å) is probably not an artifact of the calculation on the charged species ($Sn_2Se_6K_4^{2-}$), because we observe smaller $Sn-Se$ bond lengths (2.64 Å) in a calculation on the same species, in the unsymmetrical geometry of Figure 7. The elongation of the $Sn-Sn$ distances, in both the charged species to around 3.85 Å, could possibly be an artifact of the charge on the model.

In Appendix 2 we explore another way of resolving the computational problems posed by $Sn_2Se_6^{4-}$. This is by calculating some protonated models, $Sn_2Se_2(SnH)_4^{0,2-}$. The results complement the discussion here.

On balance, we thought at this point in our study that the extended structures are likely Sn^{4+}/Sn^{4+}. The computed $Se_a-Sn-Se_a$ angle of 144°, which could be due to electrostatic interactions between the K^+ ions and axial seleniums, is a matter of concern. And, as we will see below, there may be other reasons for the opening of these angles.

2. An Extended Hückel Orbital Analysis of Binding in $Sn_2Se_6^{4-}/Sn_2Se_6^{6-}$. In the DFT models for $(Sn_2Se_6)^{4-,6-}$ studied above, we encountered a classical, "tetrahedral" geometry for **8a**, and an unusual range of geometries between **8b** and **8c** (Figure 8).

In order to gain a better understanding of what happens we went over to extended Hückel (eH) calculations. A scan of the potential energy surface showed similarities between extended Hückel and DFT energies. For the "hydrogenated" models (Appendix 2) in particular, one orbital (the HOMO
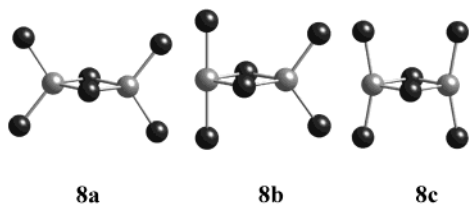
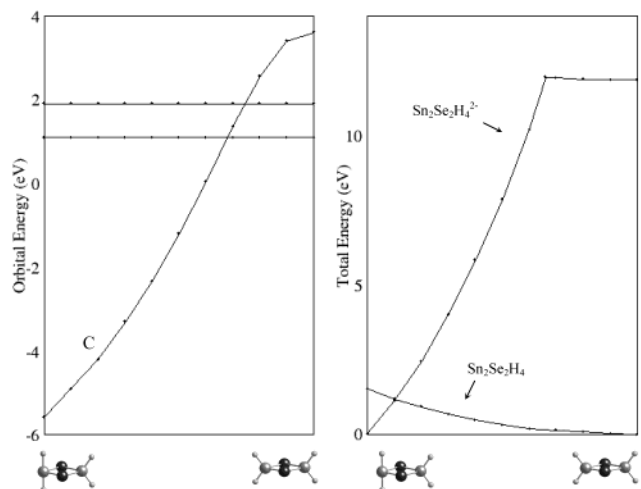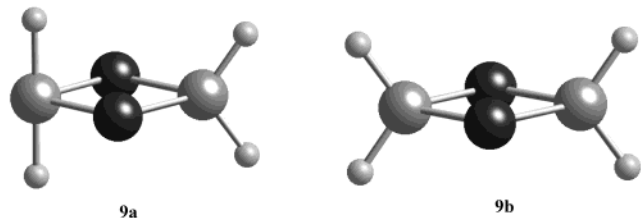**Figure 8.** Possible geometries for $(Sn_2Se_6)^{4-,6-}$ systems.

Figure 9. A Walsh diagram for a transition from **9a** to **9b**. Orbital levels are shown on the left and total energies on the right. The orbital marked C is occupied in the dianion. The horizontal axis marks a linear transit from geometry **9a** to **9b**.

of $Sn_2Se_6H_4^{2-}$) is much lower in energy for geometries **8b** and **8c** compared to **8a**.

To see the nature of the orbital involved, and why it behaves the way it does, we went back to a still simpler model in the extended Hückel calculations, replacing the terminal SeH groups by hydrogens.

Figure 9 shows a Walsh diagram for $Sn_2Se_2H_4^{0,2-}$, for a distortion in which one tin center is transformed from a hypervalent, SF_4-like geometry, to a tetrahedral geometry, **9a** to **9b**.

The orbital marked C in the figure is empty for $Sn_2Se_2H_4$ ($Sn^{4+}-Sn^{4+}$) and filled for $Sn_2Se_2H_4^{2-}$ ($Sn^{2+}-Sn^{4+}$). The change in energy is what makes geometry **9a** preferred for the 2− species. Orbital C is shown in Figure 10; it looks like a tin lone pair, with contributions from axial hydrogens.

Given the quite localized appearance of orbital C (Figure 10), we examined a C_{2v} to T_d (**11a** to **11b**) distortion at one Sn center, on a model $SnSe_4H_4^{2-}$ and the even simpler SnH_4^{2-}.[19,20]

(19) Chen, M. M. L.; Hoffmann, R. *J. Am. Chem. Soc.* **1976**, *98*, 1648−1655.
(20) Radius, U.; Silverio, S. J.; Hoffmann, R.; Gleiter, R. *Organometallics* **1996**, *15*, 3737−3745.
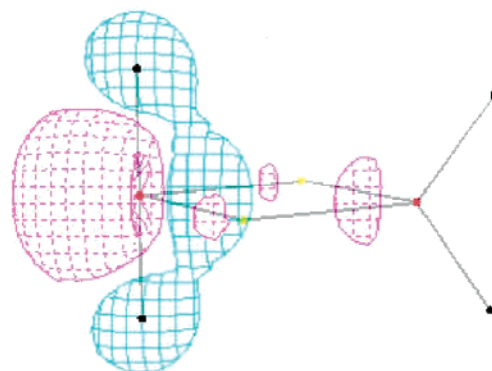
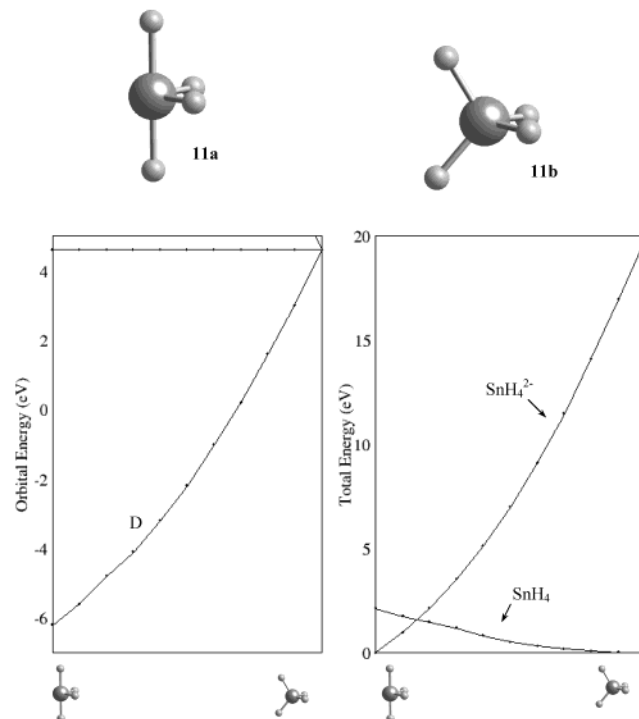**Figure 10.** Molecular orbital C; the HOMO of $Sn_2Se_2H_4^{2-}$ ($Sn^{2+}-Sn^{4+}$).

Figure 11. A Walsh diagram for a transition from **11a** to **11b**, for a Sn−H distance of 1.6 Å. Orbital levels are shown on the left and total energies on the right. Energies are in eV. The horizontal axis marks a linear transit from geometry **11a** to **11b**.
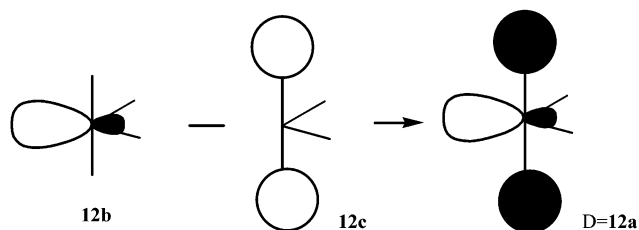

Figure 12. D is the HOMO of SnH_4^{2-} (**11a**).

The Walsh diagram for this motion for SnH_4^{2-} is shown in Figure 11. Note orbital D, the HOMO, **12a**, which goes sharply down as one approaches the hypervalent geometry (Figure 12). It looks very much like orbital C above.

Orbital D, of a_1 symmetry in point group C_{2v}, can be viewed in a number of ways. One is to see it as the antibonding mixture of the simple nonbonded hybrid **12b** at Sn with the nonbonding orbital **12c** of a classical three-center hypervalent axial orbital set.
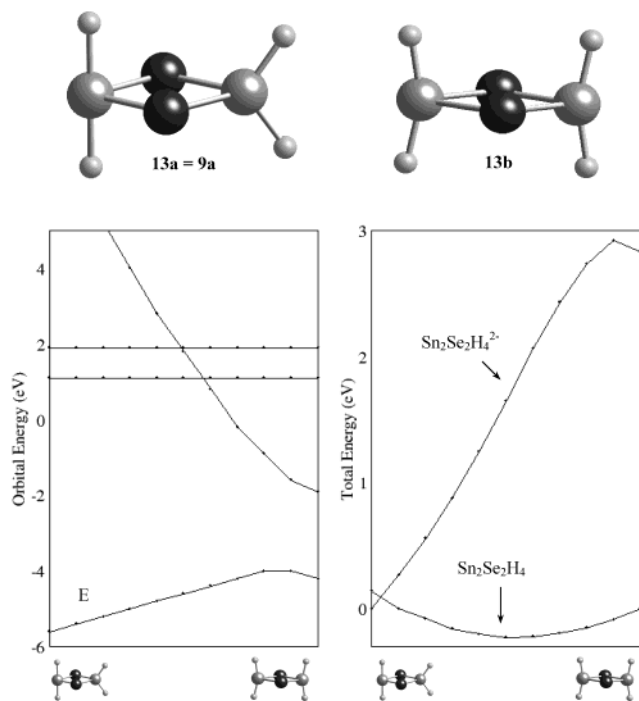
Figure 13. A Walsh diagram for a transition from **9a** to **13b**. Orbital levels are shown on the left and total energies on the right.

It is clear that **12a** is destabilized as one approaches a tetrahedral geometry. And this tendency is then incorporated into the more complex $Sn_2Se_6^{4-/6-}$ systems.

We still need to explain the potential surface of our original model relating **8b** and **8c**; a Walsh diagram for a transit between the structures **13a** and **13b**, similar to **8b** and **8c**, is shown in Figure 13.

The HOMO (E) of $Sn_2Se_2H_4^{2-}$ in **13a** starts out as the previously shown MO C (Figure 10) and goes up in energy. The rise is nowhere as steep as in the previous figures but is sufficient to make the analogue of structure **8b** favorable by 3 eV. A similar result was also observed using DFT calculations for $Sn_2Se_6K_4^{2-}$ and $Sn_2Se_6H_4^{2-}$ (in Appendix 2); in those models the energy differences are much smaller.

At this point we had a good understanding of the structures and energetics of molecular Sn^{4+}/Sn^{2+} and Sn^{3+}/Sn^{3+} systems. We still were left with an unresolved question: are the extended system Sn_2Se_6 units Sn^{4+}/Sn^{2+} or Sn^{4+}/Sn^{4+}? To approach this problem we carried out eH calculations of the extended structures.

3. Extended Hückel Analysis of the Extended Structures. Various sublattices of the extended $Sr_4Sn_2Se_{10}$ and $Sr_4Sn_2Se_9$ structures were analyzed using the eH method. One unit cell of $Sr_4Sn_2Se_{10}$ contains 16 $Sr^{2+}(Z = 4)$, 2 $Sn_2Se_6^{4-}$, 4 $SnSe_4^{4-}$, and 4 Se_3^{2-} subunits (here we make the provisional $Sn^{4+}-Sn^{4+}$ assignment in the $Sn_2Se_6^{4-}$ subunit). Similarly a unit cell of $Sr_4Sn_2Se_9$ contains 16 Sr^{2+} cations and anionic subunits of 2 $Se_2Sn_6^{4-}$, 4 $SnSe_4^{4-}$, and 4 Se_2^{2-}.

The left side of Figure 14 shows the density of states (DOS) of isolated Se_3^{2-}, $SnSe_4^{4-}$, and $Sn_2Se_6^{4-}$ sublattices. Separate calculations were also performed on isolated molecular models, and these (not shown here) reveal that

the sublattice bands are essentially those of isolated molecules, interacting very weakly. The narrow DOS peaks shown in Figure 14 testify to this.

Next we carried out a calculation on the entire $Sn_8Se_{40}^{32-}$ ($\equiv (Se_3^{2-})_4(SnSe_4^{4-})_4(Sn_2Se_6^{4-})_2$) sublattice. The right-hand side of Figure 14 shows the contributions of (top to bottom) Se_3^{2-}, $SnSe_4^{4-}$, and $Sn_2Se_6^{4-}$ sublattices to the total DOS of the $Sn_8Se_{40}^{32-}$ anionic lattice. At first glance it would seem there is little interaction between the sublattices. But, the "movement" of the $Sn_2Se_6^{4-}$ subunit's first and second unfilled bands provides a clue to the contrary. These unfilled bands (near -5 eV) are pushed up (to near -2 eV) in the composite anionic lattice, indicating that they are interacting with the lower levels. The Se_3^{2-} subunit has a band lower than -5 eV which is unoccupied but this does not interact with the $Sn_2Se_6^{4-}$ bands, because it is unperturbed in the total anionic DOS structure. One or more levels from the rest of the bands lower than -5 eV ($Sn_2Se_6^{4-}$) band, which are all occupied, may be involved in the above interaction. We expect that such interactions will populate the LUMO and LUMO+1 of $Sn_2Se_6^{4-}$.

A fragment molecular orbital (FMO) analysis indicates in fact that the $Sn_2Se_6^{4-}$ LUMO and LUMO+1 together acquire (are populated by) 0.41 and 0.31 electrons in the $Sn_8Se_{40}^{32-}$ and $Sn_8Se_{36}^{32-}$ sublattices derived from $Sr_4Sn_2Se_{10}$ and Sr_4-Sn_2Se_9.

From where does this electron transfer occur? An examination of the structure (Figure 16) reveals that each $Sn_2Se_6^{4-}$ unit in the lattice has intermediate range secondary $Sn-Se$ interactions with four neighboring $SnSe_4^{4-}$ molecules; these are shown by dotted lines. The result is that for each Sn center there are two further Se contacts. In $Sr_4Sn_2Se_{10}$ these contacts are 3.12 and 3.42 Å; and in $Sr_4Sn_2Se_9$ both are 3.33 Å.

There is no indication that the electrons are transferred from Se_2^{2-}/Se_3^{2-} subunits to a $Sn_2Se_6^{4-}$ subunit. The evidence for this is 2-fold. First, from the DOS in Figures 14 and 15, the Se_2^{2-}/Se_3^{2-} levels are not perturbed. This indicates minimal interactions of Se_2^{2-}/Se_3^{2-} subunits with the other anionic subunits. Second, we looked in the structure for any sign of possible oxidation of Se_2^{2-} and Se_3^{2-} subunits. The Se$-$Se distances in Se_2^{2-} and Se_3^{2-} sublattices are 2.45 and 2.40 Å, respectively. These distances are longer than the Se$-$Se single bond distance in elemental Se_∞, which is 2.37 Å.[21] The Se$-$Se bond length in Se_2^{2-} units contained in simple lattices of Na_2Se_2, K_2Se_2, Rb_2Se_2, and $BaSe_2$ are 2.38 Å, 2.40 Å, 2.47 Å and 2.33 Å, respectively.[22-24] The Se_3^{2-} subunits in K_2Se_3, Rb_2Se_3, Cs_2Se_3, and $BaSe_3$ have two equal Se$-$Se bonds. They measure 2.38 Å, 2.37 Å, 2.35 Å, and 2.35 Å, respectively.[24,25] The Se$-$Se$-$Se angle in

(21) Greenwood, N. N.; Earnshaw, A. *Chemistry of The Elements*; Pergamon Press: Oxford, 1990; p 897.
(22) Föppl, H.; Busmann, E.; Frorath, F. K. *Z. Anorg. Allg. Chem.* **1962**, *314*, 12−29.
(23) Böttcher, P.; Getzschmann, J. *Z. Anorg. Allg. Chem.* **1993**, *619*, 476−488.
(24) Hulliger, F.; Siegrist, T. *Z. Naturforsch., B: Chem. Sci.* **1981**, *36*, 14−15.
(25) Böttcher, P. *Z. Anorg. Allg. Chem.* **1977**, *432*, 167−172.
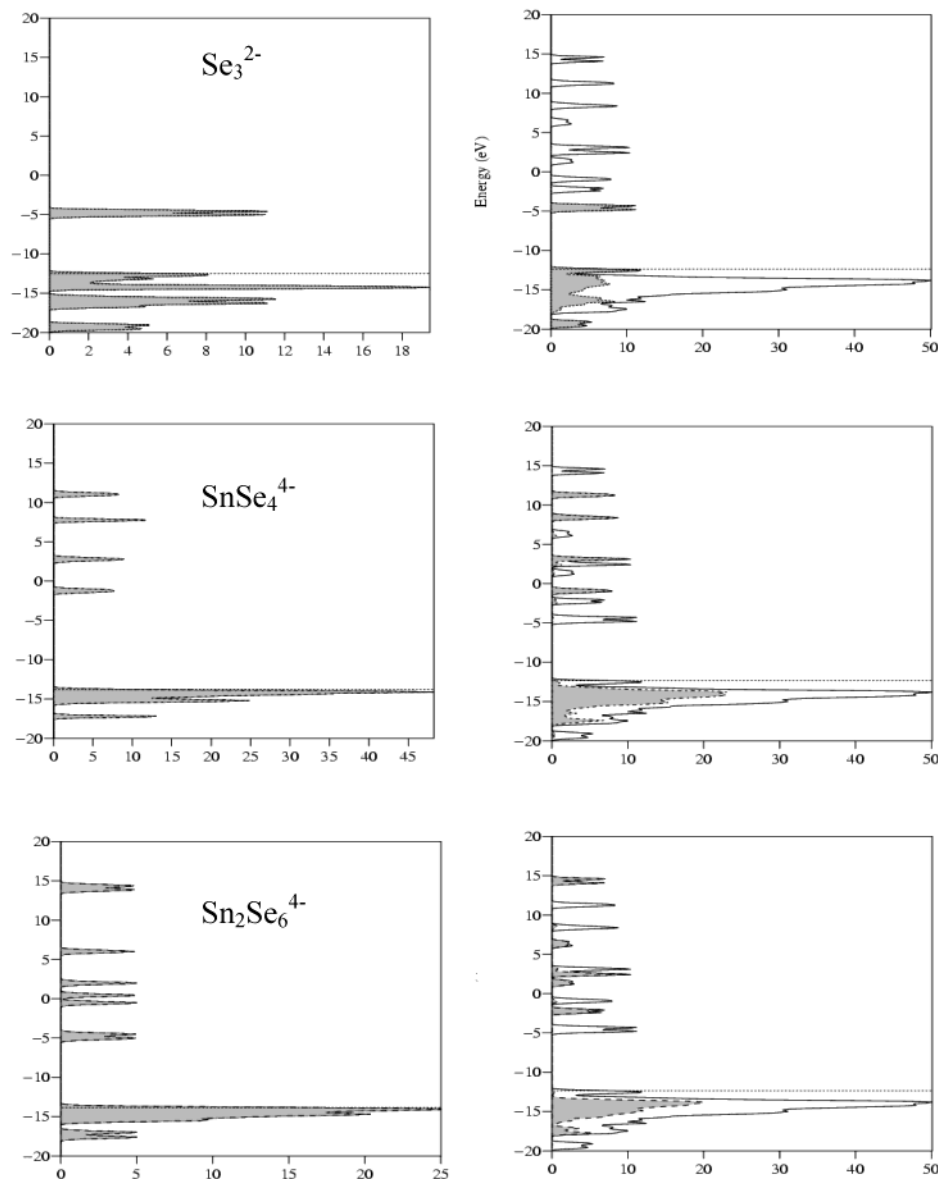
Figure 14. Left side of the figure shows the DOS of isolated Se_3^{2-}, $SnSe_4^{4-}$, and $Sn_2Se_6^{4-}$ sublattices from top to bottom. The right side shows the contributions of respective sublattices to the total DOS of the $(Sn_8Se_{40})^{32-}$ anionic lattice.

K_2Se_3, Rb_2Se_3, Cs_2Se_3, and $BaSe_3$ are 102°, 103°, 103°, and 111°, respectively. Se_3^{2-} in $Sr_4Sn_2Se_{10}$ has a Se−Se−Se angle of 108°, which lies in this range. Were the Se_2^{2-} or Se_3^{2-} oxidized, the Se−Se bond length should be shorter, as some multiple bonding would ensue. This is not seen.

Now the oxidation state assignment becomes a little murky. Looking at just the levels and bands, it would seem that the Sn_2Se_6 sublattice in $Sr_4Sn_2Se_{10}$ and $Sr_4Sn_2Se_9$ is 4− and not 6−. To have a $Sn_2Se_6^{6-}$ sublattice one would need to occupy what in the isolated molecule/sublattice would be level(s)/band(s) which are 8−10 eV above the Fermi level. And yet there is some population in the extended structure of $Sn_2Se_6^{4-}$ LUMOs, through secondary interactions.

A Related Structure. Another compound, $Eu_8(Sn_4Se_{14})$-$(Se_3)_2$ (Figure 17), which is structurally similar to Sr_4Sn_2-Se_{10}, has also been recently reported.[26] $Eu_8(Sn_4Se_{14})(Se_3)_2$ has a $Sn_4Se_{14}^{12-}$ building block (Figure 18). This can be thought as composed of three subunits: one $Sn_2Se_6^{4-}$ and

two $SnSe_4^{4-}$, which are connected by two long Sn−Se bonds (3.03 Å), are shown in Figure 18. There is also a 3.32 Å Sn−Se contact, between adjacent $Sn_4Se_{14}^{12-}$ subunits; this is indicated in Figure 18 by dashed lines.

The tin centers in the Sn_2Se_6 subunits are thus effectively coordinated to six selenium atoms, if we include the Se atoms with the dotted contacts in the coordination sphere (Figures 16 and 18). The environment is a distorted octahedron, shown in Figure 19. The distortion may be described as primary elongation of two cis equatorial bonds. How can this distortion be understood?

4. Distorted $SnSe_6^{n-}$ Octahedron. Assuming a Sn^{4+} surrounded by 6 Se^{2-}, we have at hand a 12-electron main group octahedral $SnSe_6^{8-}$ species. Were the Sn 2+, we would have a 14-electron $SnSe_6^{10-}$.

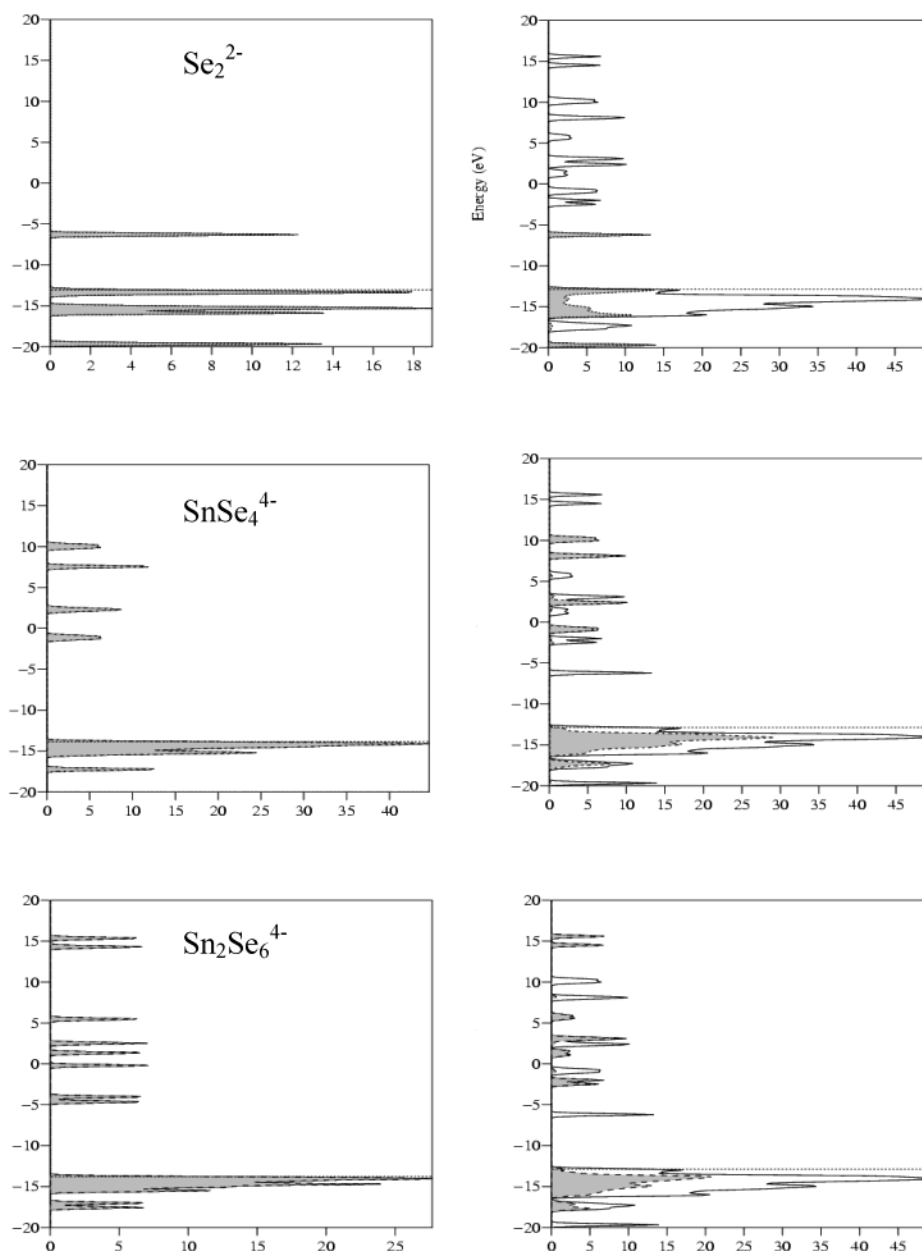(26) Evenson, C. R., IV; Dorhout, P. K. *Z. Anorg. Allg. Chem.* **2001**, *627*, 2178−2182.

Figure 15. The left side of the figure shows the DOS of isolated Se_2^{2-}, $SnSe_4^{4-}$, and $Sn_2Se_6^{4-}$ sublattices from top to bottom. The right side shows the contributions of the respective sublattices to the total DOS of the $(Sn_8Se_{36})^{16-}$ anionic lattice.

VSEPR theory predicts that 14-electron octahedral species, with six bond pairs and one lone pair of electrons, will distort.[27,28] In such a case the bonds close to the lone pair should be elongated. An MO picture also leads to a similar scenario, as we describe below.[29]

Figure 20 shows at left the construction of the orbitals of a 14-electron octahedral main group AL_6 compound.[29] The ordering of the $a_{1g}*$ and $t_{1u}*$ higher-lying orbitals is from an eH calculation. This system is set up for a second-order Jahn Teller distortion, as a consequence of the proximity of $a_{1g}*$

and $t_{1u}*$ orbitals. Figure 21 focuses in on what happens to the upper levels.

In Figure 21 we see the HOMO α for the 14-electron octahedral species; it is an antibonding a_{1g} MO. On elongating two $Sn-Se_c$ bonds, i.e., lowering the point group symmetry from O_h to C_{2v}, α and one component of t_{1u} in O_h symmetry can mix, because both orbitals now have the symmetry a_1. The result of the mixing is a lower energy HOMO, β.

An eH calculation indicates that the total energy and the energy of the HOMO of the $SnSe_6^{10-}$ octahedral molecule are lowered on elongating the $Sn-Se_c$ bonds from 2.6 to 3.3 Å.

MO β also indicates that the $Sn-Se_{ax}$ bond elongation could accompany the distortions described above for a 14-

(27) Sidgwick, N. V.; Powell, H. M. *Proc. R. Soc.* **1940**, *A176*, 153−180.
(28) Lawton, S. L.; Fuhrmeister, C. J.; Hass, R. G.; Jarman, C. S.; Lohmeyer, F. G.; *Inorg. Chem.* **1974**, *13*, 135−143.
(29) Gimrac, B. M.; Liebman, J. F.; Kohn, M. *J. Am. Chem. Soc.* **1978**, *100*, 2334−2339.
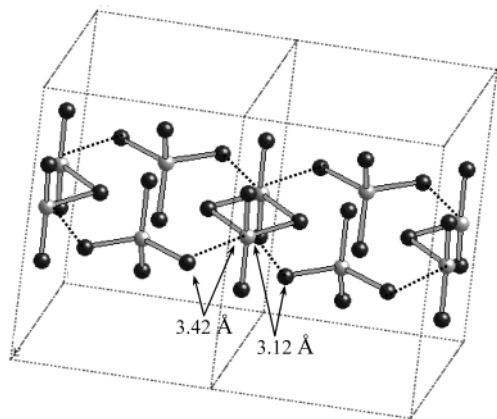
Figure 16. The arrangement of the $SnSe_4^{4-}$ and $Sn_2Se_6^{4-}$ subunits in $Sr_4Sn_2Se_{10}$ can be seen. The contacts between these subunits are shown by dotted lines. Both the distances shown are equal in $Sr_4Sn_2Se_9$ (3.33 Å).

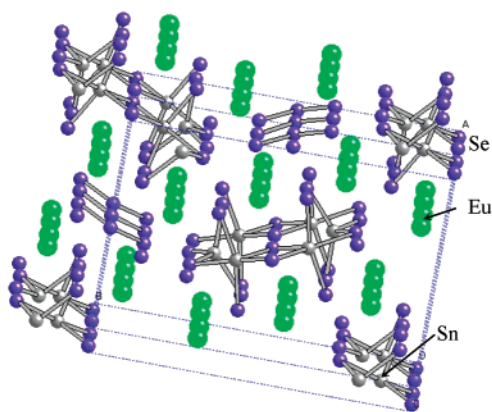**Figure 17.** $Eu_8(Sn_4Se_{14})(Se_3)_2$ has a structure similar to $Sr_4Sn_2Se_{10}$ and $Sr_4Sn_2Se_9$, which are shown in Figures 3 and 4.
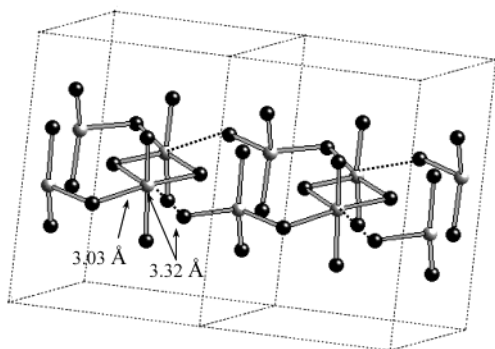
Figure 18. $Sn_4Se_{14}^{12-}$ subunit of $Eu_8(Sn_4Se_{14})(Se_3)_2$ can be seen here as one $Sn_2Se_6^{4-}$ and two $SnSe_4^{4-}$ molecules linked with long 3.03 Å bonds. Dashed lines show secondary bonding contacts of 3.32 Å.

electron species ($SnSe_6^{10-}$), because the MO components on Se_{ax} and Sn of MO β resemble the HOMO of a hypervalent, electron rich three-center system (Figure 12a). It is the antibonding character of this occupied MO that leads to the bond elongation.

These bond elongations (axial and cis-equatorial) are experimentally observed in isoelectronic $SbCl_6^{3-}$.[30] Actually, there are many structures with this counterion. The distortions observed are complex and of several types; the reader is

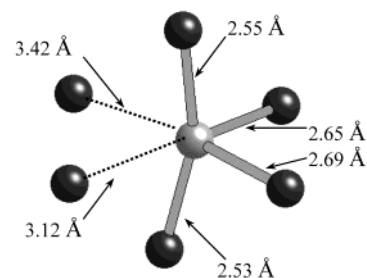(30) Knodler, F.; Ensinger, U.; Schwarz, W.; Schmidt, A. *Z. Anorg. Allg. Chem.* **1988**, *557*, 208−218.

Figure 19. A distorted octahedron in the crystal structure of $Sr_4Sn_2Se_{10}$.
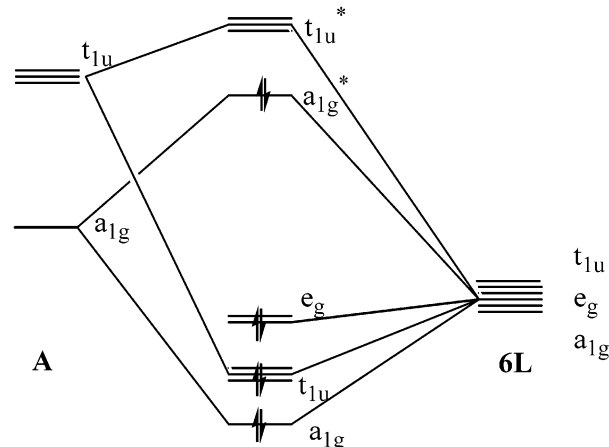

Figure 20. Molecular orbitals of a 14-electron AL_6 compound.
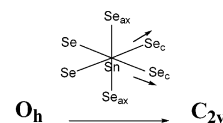

Figure 21. Octahedral to C_{2v} distortion in a 14-electron species ($SnSe_6^{10-}$). Note: HOMO and higher orbitals are shown in this picture.

referred to the analysis of pseudo Jahn−Teller distortions in XeF_6 for an appreciation of the complexity of the problem.[31]

We do not observe the axial bond lengthening in Sn_2Se_6 subunits of the Pocha and Johrendt structure;[2] the Sn−Se_a bond lengths are 2.51−2.55 Å, which are in the range seen for normal Sn−Se bonds. Trusting these distances, we think the distortion seen in Figure 19 may not be a consequence of 14-electron AL_6 complex. Hence, the association of 2+ oxidation state (which for a while seemed appropriate), to the tins in question is not likely.

Similar elongation of the Sn−Se_c bonds is not observed in 12-electron octahedral species by MO analysis. VSEPR

(31) Wang, S. Y.; Lohr, L. L. *J. Chem. Phys.* **1974**, *60*, 3901−3915.

Table 1. Extended Hückel Parameters[18]

atom	orbital	H_{ii}	ζ_1
Sn	5s	−16.16	2.12
	5p	−8.32	1.82
Se	4s	−20.50	2.44
	4p	−14.40	2.07
H	1s	−13.60	1.30
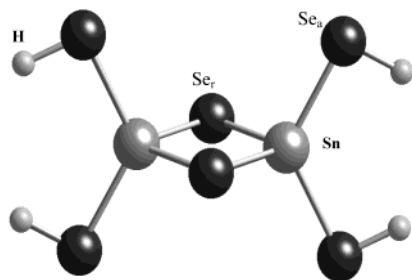
Figure 22. The optimized computed structure for $Sn_2Se_6H_4$.

theory does not predict a distortion for a 12-electron species, which has six bond pairs, from a regular octahedron. This analysis, like the others, does not yield a conclusive answer.

Conclusions

Usually the oxidation state correlates with a system's structure and electronic properties. But the tins in the extended Pocha and Johrendt Sn_2Se_6 sublattices, which were assigned a formal 4+ oxidation state, show some geometrical properties inconsistent with the assignment. The geometry around tins does not resemble either classical Sn^{4+} or Sn^{2+}. Assignment of an intermediate oxidation state for tin in the Sn_2Se_6 subunits, Sn^{3+}, would be in disagreement with the formal charge of the Sn_2Se_6 subunits in the lattice. And there is no sign that any element of the remaining lattice is oxidized. Hence, we suggest that, on balance, Sn^{4+} is still an appropriate description of the tins in Sn_2Se_6 subunits.

The structural peculiarities of the Sn^{4+} centers in the reported structures may be traced back to the inter-sublattice interactions, between the $SnSe_4$ and Sn_2Se_6 sublattices.[2]

Appendix 1

See Table 1.

Appendix 2

Hydrogenated $Sn_2Se_6^{4-}$ Models. The computational problem with $Sn_2Se_6^{4-}$ could be approached in another way, by adding four protons to the axial seleniums, leading to $Sn_2Se_6H_4$ as a model for the Sn^{4+}/Sn^{4+} system.

When the geometry of $Sn_2Se_6H_4$ was optimized, we obtained the structure shown in Figure 22 (confirmed computationally to be a minimum). The angle $Se_a-Sn-Se_a$, which is 122°, is within the experimentally observed range of angles (104−127°) (for normal Sn^{4+} compounds). The
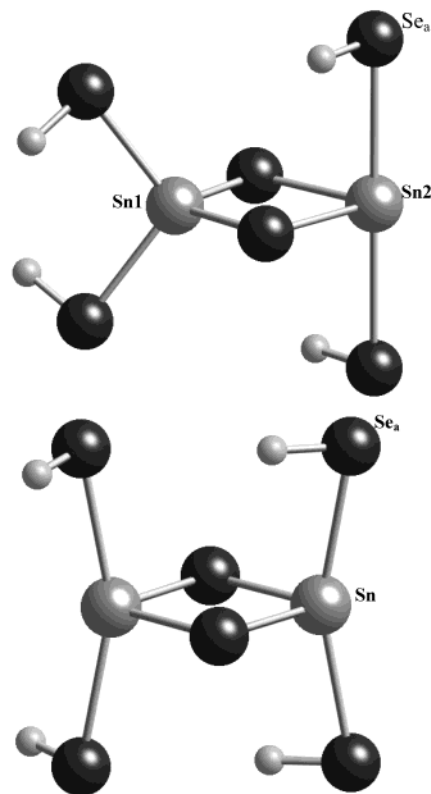
Figure 23. (a) One of the computed structures for $Sn_2Se_6H_4^{2-}$. (b) The second and interesting structure for $Sn_2Se_6H_4^{2-}$.

computed Se_a-Sn distance is 2.65 Å, and the $Sn-Sn$ distance is 3.47 Å. These characteristics are very similar to those of the typical Sn_2Se_6 subunit in extended structures.

We next wanted to model the $Sn^{3+}-Sn^{3+}$ system. The symmetrical $Sn_2Se_6H_6$ model that suggests itself, with one hydrogen per selenium, unfortunately fragments to $Sn(SeH)_4$ and $Sn(SeH)_2$. This is by itself interesting, demonstrating the stability of group IV carbenoid structures, but is not relevant to our problem. We next tried $Sn_2Se_6H_4^{2-}$, protonating only the terminal seleniums, and obtained two apparent minima. The molecules actually had imaginary frequencies less than 30 cm^{-1}, likely derived from low energy hydrogen motion.

One of the geometry-optimized structures of $Sn_2Se_6H_4^{2-}$ is A (Figure 23a), which indeed has different environments for the tins. In the computed optimum structure the $Se_a-Sn1-Se_a$ is 179° and $Se_a-Sn2-Se_a$ is 106°. The $Sn1-Sn2$ distance is 3.70 Å, which is elongated compared to the protonated $Sn^{4+}-Sn^{4+}$ model. Perhaps this is due to the uncompensated charge on the model. $Sn2-Se_a$ and $Sn2-Se_r$ are 3.15 and 2.92 Å, respectively; they are longer than $Sn1-Se_a$ and $Sn1-Se_r$, which are 2.76 and 2.51 Å, respectively. The structure certainly resembles the mixed-valence compound discussed earlier.

The other structure obtained for $Sn_2Se_6H_4^{2-}$, B (Figure 23b), is interesting because it has both the tins in similar environments. The computed $Se_a-Sn-Se_a$ angle is 159°, and the structure is similar to the unusual Sn_2Se_6 subunit[2] observed in extended structures. The $Sn-Se_a$ distance of 2.98 Å, however, is greater than the distance observed in the

unusual subunit (2.51−2.55 Å). The energy of this structure is 0.4 eV greater than that of its isomer A.

Is there a barrier between A and B? To probe this, we computed a linear transit between A and B, gradually varying the Se_a−Sn−Se_a angles. During each step the geometry is partially optimized, keeping the Se_a−Sn−Se_a angles fixed.

We find no barrier going from A to B. This is an indication that B probably is a transition state for interchanging Sn-(II)−Sn(IV) environments.